Coupling Models and Data: which possibilities for remotely-sensed images?

Isabelle Herlin[1], François-Xavier Le Dimet[2], Etienne Huot[1] and Jean-Paul Berroir[1]

[1] INRIA Rocquencourt - CLIME project
Isabelle.Herlin@inria.fr, Etienne.Huot@inria.fr,
Jean-Paul.Berroir@inria.fr
BP 105
78153 Le Chesnay CEDEX
France
[2] INRIA - IDOPT project
Francois-Xavier.Le-Dimet@imag.fr
LMC-IMAG
51 rue des Mathématiques
B. P. 53
38041 Grenoble Cedex 9
France

Abstract. The international scientific context is pointing out the role that can be played by models and observation systems for the evaluation and forecasting of the risks related to environmental problems.
In this context, coupling data and models becomes a scientific challenge regarding the following considerations: A numerical model without observation data is not really interesting; On the other hand models lack the necessary data for forecasting, since they require an accurate initial condition for expecting good results and are making use of parameters which can not be obtained by measurement, for example sub-mesh parameterization. There is thus a need for an optimal use of all the available information, in order to constraint as best as possible models with their input data and parameters.
Data assimilation (variational methods or Kalman filters) is a solution for combining different types of information: data and models. However structured spatial information of images are not often used in this context. If they are, this is in a qualitative way and not with accurate quantitative information.
This paper is then considering the problem of Image Data Assimilation by focusing on satellite acquisition and on oceanographic applications. It is evaluating the different quantitative measures that could be obtained on these data for assimilation within these models.

1 Introduction

The international scientific context is pointing out the role that can be played by models and observations systems for the evaluation and forecasting of the

risks related to environmental problems. International research programs such as GMES (Global Monitoring for Environment and Security) have been created to focus on this point.

In this context, coupling data and models becomes a scientific challenge regarding the following considerations: a numerical model without observation data is not really interesting, and the available observations are not sufficient for forecasting. This is especially the case of geophysical models, that are highly non-linear and thus require a very accurate knowledge of the initial condition. Furthermore, mathematical models are making use of internal parameters (such as sub-mesh parameterization) which can not be obtained by measurements. There is therefore a need for techniques to make an optimal use of the available of information, in order to constraint models as best as possible with an unsufficient input data set (observation data and parameters).

Data assimilation is a mathematical solution for combining different types of information: data and models. However images, when used in a data assimilation framework, are either used in a qualitative way, or considered as data with no spatial coherence as a collection of individual measurements.

This paper aims at discussing the potential of remotely-sensed images for assimilation within environmental models with specific application to oceanography. What is interesting is first to determine the different types of information available in satellite acquisition, and then to examine how to perform data assimilation with these information.

Section 2 shortly discusses the general problem of data assimilation and describes the model we are using in this paper to illustrate our research. This section also defines the different types of information which should be extracted from static images or from image sequences.

Section 3 describes in 3.1 the available satellite data for oceanographic studies and summarize their properties. Then subsection 3.2 focus on the problem of motion estimation: how to obtain good results of apparent motion by taking into account the available information about data acquisition and observed processes? Results are analyzed by using synthetic data produced by a given oceanographic circulation model. The final aim is to obtain a good quality motion field which should be assimilated in the model. Subsection 3.3 is then discussing the problem of structure detection. This can be performed on a static image or it can be done on a temporal sequence by tracking the deformable structure in time. It is then possible to compute the Lagrangian trajectories of these structures and compare them to in situ data (for instance ARGOS drifters) in order to perform assimilation of Lagrangian data.

2 Data Assimilation within oceanographic models

Data assimilation is a global mathematical framework for combining heterogeneous information: data and mathematical model equations, in order to restore as best as possible the state variables of the model. It has first been used in meteorology with huge numerical models (6 millions of variables) [21], and then in

hydrological [19, 31] and oceanographic applications[7, 14]. But this is a general framework used in other domains: air pollution, biomedical applications, ... Up to now two main technical approaches of data assimilation have been developed:

- Sequential methods based on Kalman filtering,
- Variational methods based on optimal control.

Data used for assimilation are usually direct or indirect measurements of model's state variables. In this context, images and particularly oceanographic satellite data, contain a lot of information, which should be useful for the control of models and are yet not used enough. A good example is provided by the meteorological domain: there is a huge amount of available satellite data (approximatively 20 space-borne sensors are dedicated to meteorological applications, 11 of which being operational and constituting the World Meteorological Organization's Global Observation System). There satellite data can be assimilated as a collection of individual measurements (ex: each infrared pixel considered as a local measure of temperature), but the **structured spatial information** observed on these images is used in a rather qualitative way, although techniques inspired from computer vision can be applied for that purpose: for example, the detection of dark structures on water vapor images conducts to the correction of forecast in case of storms by running again the model with different initial conditions [29]. Then the interesting question is: how to make use of the quantitative structured information contained in satellite data to better predict the state of a system?

For clarity, we discuss this problem in the case of variational assimilation and for oceanographic applications. It corresponds to the set of following equations:

$$\begin{cases} \dfrac{dX}{dt} = F(X, K) \\ \\ X(0) = V \\ \\ J(V, K) = \dfrac{1}{2} \displaystyle\int_0^T \|CX - X_{obs}\|^2 dt. \end{cases} \tag{1}$$

where:

- X denotes the state vector corresponding to the output of the model,
- K denotes the control parameters of the model,
- F is the model forecast operator,
- V denotes the initial (background) condition at date $t = 0$,
- J is a cost function taking into account the difference between the prediction of the model and the observation X_{obs},
- C is the observation operator going from the space of state variables to the space of observation.

The challenge is to add a term allowing to compare the image acquisitions to the state variables of an oceanographic model, which requires the definition of a new operator from the space of state variables to the space of images, or to the space of image characteristics. This problem gives rise to different considerations:

– On the image content: images can be static and in this case we should consider structures as explained in subsection 3.3, or they can be dynamic and in this case we can be interested either by motion estimation (subsection 3.2) or by Lagrangian trajectories of structures (subsection 3.3).
– On the image space: choice of mathematical spaces adapted to represent boundaries of structures, Lagrangian trajectories, motion fields, *etc.*
– On the operator going from the state vector space to the image space.
– On the regularity of the image space: it is necessary to add a regularity term in the image cost function, since information extraction from images is often an ill-posed problem.

Coming to the problem of assimilation of dynamic data obtained from satellite images (which is the most interesting problem regarding the oceanographic application), we are facing different possibilities, which will be discussed in this paper:

– Assimilation of a motion vector field, which corresponds to a state variable of an oceanographic model,
– Assimilation of Lagrangian trajectories obtained by detection and tracking of characteristic deformable structures,
– Assimilation of Lagrangian trajectories obtained by temporal integration of a motion vector field.

As surface velocity is a state variable of ocean circulation models, direct Eulerian assimilation of this information is possible. Satellite acquisitions allow to observe the ocean surface. We try to infer the surface apparent motion from these observations. But velocity estimation is prone to errors as we will extensively discuss in this paper. Using trajectories could be interesting because it completes the assimilation system with the variables corresponding to Lagrangian data. There are two main interests in trajectories: the determination of these trajectories often rely on alternative image techniques such as structure detection and tracking. Moreover, buoy drifter data are available for validation.

For better focusing our paper and defining which data we will be able to use for assimilation, we discuss our ideas with a specific ocean circulation model called OPA, a 3D primitive equation model developed by LODYC [23]. This model ran in the North-East Atlantic configuration with a spatial resolution of 0.05^o and a daily temporal resolution over 3 months. The state variables of the model are the velocity $\mathbf{w}_M = (u_M, v_M, w_M)$ at different vertical layers, temperature and salinity; the chlorophyll concentration can also be derived by coupling the biological model LOBSTER [15]. The input data, or control variables, are the initial conditions of the state variables and the boundary conditions (surface, wind stress, friction, radiative forcing). The model has been calibrated in order to provide an integrated view of the evolution of the spring bloom during the Program of Ocean Multidisciplinary MEsoscale (the POMME campaign)[22]. The domain of interest covers the location of the strongest large scale meridional gradient in wintertime mixed-layer depth. In this way, we obtain two synthetic sequences of 88 images with size 99 lines by 109 columns representing respectively

the surface temperature and chlorophyll concentration, these are associated to a sequence of 99×109 vector images representing the motion field at the surface, with its two components $\mathbf{w}_M = (u_M, v_M)$.

As it will discussed in section 3, the outputs of the OPA model (temperature, chlorophyll) are comparable to information provided by oceanographic satellites, in terms of data nature, spatial and temporal resolution, but free of cloud and atmosphere contamination. Furthermore, the OPA model provides a velocity field consistent with the temperature and chlorophyll data: this is of course not available in practice with satellite data, and provides us with a powerful validation framework since we will be able to check the estimated apparent motion against the OPA motion field. The OPA motion fields will be furthermore used to check the validity of different mathematical models (such as conservation equations) we apply on image data

Before getting to motion and trajectories estimation in the next section, we first present the current state-of-the-art of satellite images dedicated to oceanography and their potential for data assimilation.

3 Analysis of the potential of satellite data for assimilation

Satellite data and their qualitative and quantitative content will be presented in subsection 3.1. Different problems can be considered for coupling satellite data and oceanographic models, that will then be discussed in the following subsections. First we consider the estimation of apparent motion on oceanographic satellite images (subsection 3.2). Physical information on data acquisition and on oceanography has to be used to derive adequate conservation and regularity constraints for the numerical estimation process. We then show results of motion estimation validated against synthetic velocity fields. Finally, structure segmentation and tracking in order to compute Lagrangian trajectories is presented in subsection 3.3.

3.1 Satellite data

For oceanographic applications, we can make use of two main types of image data in order to study the problems of motion and structures detection and tracking: Sea Surface Temperature images and Color data. We do not mention other satellite data, which are not acquired as images (such as along-track scanners), for which images are produced after interpolation of the different satellite tracks: this is for instance the case of altimetry (Topex-Poseidon, Jason), scatterometer (NSCAT, Seawinds). We also do not address in this study SAR images used for monitoring polar ice and oil-spills.

– SST data are acquired from thermal imagery in the infrared domain, and are very often provided by meteorological satellites. SST estimation rely on the analysis of brightness temperatures, obtained by inverting the Planck

blackbody function from the radiance measurements, and by combining different infrared channels so as to discard the contribution of atmosphere to the signal. SST data can be accessed on a global scale using geostationary platforms (Meteosat, GOES, GMS, ...), with continuous acquisition every 15 or 30 minutes, but coarse spatial resolution (5 to 20km). Polar orbiting platforms, such as NOAA-AVHRR, MODIS or the future MetOp satellites, provide information at synoptic scale with daily revisit and a spatial resolution ranging from 250m to 1km (see example images on figure 1).
- Ocean color data are acquired in the visible spectrum, using channels narrowed on chlorophyll absorption bands, and after correction of the atmosphere contribution. This product is then strongly related to concentration of phytoplankton in the near surface (first few meters) and give information on the marine biology. Ocean color is provided by sensors on-board polar orbiting satellites, thus providing mesoscale data (app 1km) with daily revisit. The main ocean color sensors are SeaWiFS and MODIS.

SST and oceanographic color images provided by space sensors have a strong potential for oceanographic applications. They make it possible to observe current patterns such as fronts, eddies, filaments, upwelling, and provide information on the oceans' biologic activities. They are well adapted to mesoscale and global studies, owing to the complementarity between geostationary and polar orbiting platforms. Their major limitations mostly concern the spatial/temporal resolution tradeoff (eg geostationary satellite provide a very dynamic information but with limited spatial information, whereas polar orbiting satellites show more spatial details but on a daily basis), which prevents the study of very local (below km) and quick (shorter than a day) phenomena. Another major limitation comes from cloud coverage, which prevents the acquisition of both visible and infrared images, and consequently ocean color and SST measurements. As a consequence, a significant part of data is hidden and not available, or partly available but with spectral signatures greatly affected by clouds.

3.2 Apparent motion on images

The problem of apparent motion computation has been extensively studied in the literature [1, 4, 5, 9, 18, 24, 28]. We consider this problem in the context of satellite data and oceanographic application in order to determine the best mathematical equations which could be used for estimating motion.

The classical approach in computer vision assumes the conservation of the grey level value for individual pixels (often called optical flow constraint). Given a pixel with coordinates $(x(t), y(t))$ on an image I at date t, we have $\frac{dI}{dt}(x(t), y(t), t) = 0$ or equivalently:

$$\frac{\partial I}{\partial x}\frac{dx}{dt} + \frac{\partial I}{\partial y}\frac{dy}{dt} + \frac{\partial I}{\partial t} = 0 \Leftrightarrow \nabla I \cdot \mathbf{w} + I_t = 0 \tag{2}$$

where ∇I is the spatial gradient, $\mathbf{w}$ is the apparent motion on the sequence, $\cdot$ denotes the scalar product, and I_t the temporal partial derivative of I. Equation

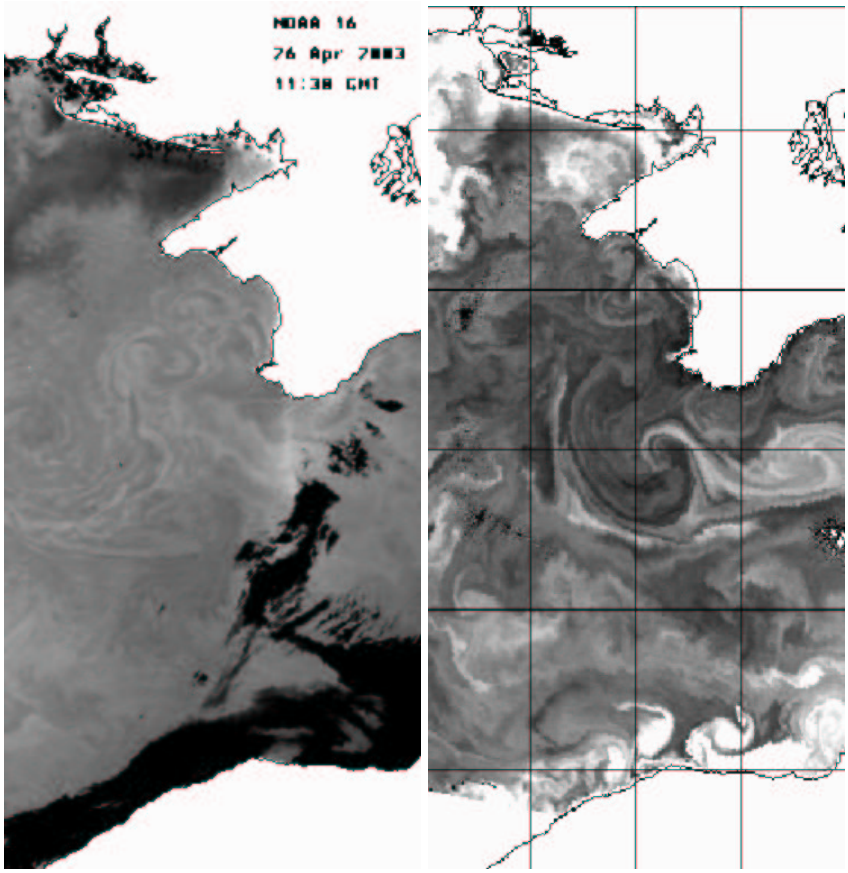

(a) (b)

Fig. 1. Part of the Black Sea. SST computed from NOAA/AVHRR (a), SST computed from MODIS (b).

(2) expresses the pixel's luminance conservation over time: moving points keep a constant brightness during their motion.

This equation has two unknowns: $\mathbf{w} = (u, v)$ and cannot be directly solved. One classical approach for constraining it in computer vision is to define an energy functional $E_1(\mathbf{w}) = \int_I (\nabla I \cdot \mathbf{w} + I_t)^2$ over the image space; then to add an additional constraint, for example a L_2 regularity for $\mathbf{w}$, and to express it within a second energy functional $E_2(\mathbf{w}) = \int_I \|\nabla \mathbf{w}\|^2$; and endly to minimize $E_1 + E_2$ to obtain an estimation of $\mathbf{w}$.

In the context of fluid motion on oceanographic images, which is quite complex with eddies, fronts and upwelling phenomena, we still keep the framework of energy minimization, and solve it with variational methods for example, but we have to further analyze the two components of the energy function to be minimized: conservation equation and regularity constraint, in order to better adapt them to the specific context of acquisition process and observed phenomena.

In order to investigate which conservation equation and regularity constraint are best verified, we use the output of the OPA ocean circulation model [23], shortly described in section 2. Our final aim is to be able to better estimate motion values on satellite data for data assimilation within such prediction models, in order to allow better forecasts. In this study we have a model output [22] corresponding to 3 months with daily values of temperature, chlorophyll and velocity at near surface (2.5m), which will be considered as surface values. The spatial and the temporal resolution of these images are similar to NOAA/AVHRR sensor acquisitions (5km^2, daily), so our conclusions could be later used on real satellite acquisitions. What is really interesting with these simulations is that we have access to the velocity field computed by the OPA model and corresponding to the image data: we can then estimate a motion field from the temperature or chlorophyll image sequences (see examples figure 2) and compare it with this model velocity field $\mathbf{w}_M$ (see example on figure 3). The motion field obtained as OPA output serves for validation of the motion estimation described in the following subsections. Our input data for the motion field estimation process will then be the SST and Chlorophyll sequences.

Which conservation equation? Apart from the luminance conservation:

$$\frac{dI}{dt}(x, y, t) = \nabla I \cdot \mathbf{w} + I_t = 0$$

the literature expresses other possible constraints. The mass conservation [6, 13, 33] is the conservation of the density for a compressible fluid, it presents one additional term on the divergence of the apparent motion vector field:

$$\nabla I \cdot \mathbf{w} + I_t + I \mathrm{div} \mathbf{w} = 0 \tag{3}$$

On SST data, we can also consider the equation governing the transport of a scalar quantity (temperature) by a fluid. It is in general an advection-diffusion equation, which gets simpler when considering the popular Boussinesq

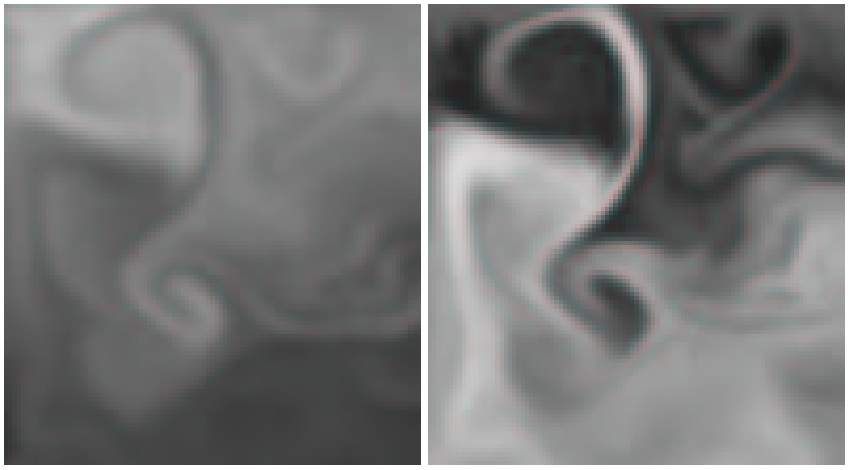

Fig. 2. Example of SST and Chlorophyll images obtained from OPA model.

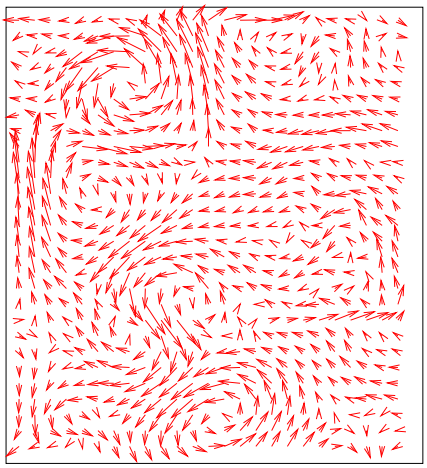

Fig. 3. Simulated motion field $\mathbf{w}_M$.

approximation, that tends to neglect the variations of water density (quasi-incompressible approximation):

$$\frac{dT}{dt} = \frac{\partial T}{\partial t} + \nabla T \cdot \mathbf{w} = K_T \Delta T \tag{4}$$

where K_T is the thermal diffusivity coefficient and Δ denotes the Laplacian operator. Notice that we should also consider source and sink terms, which occur at the ocean surface due to radiative forcing.

On color data, it is possible to apply the advection-diffusion equation to the chlorophyll concentration:

$$\frac{dC}{dt} = \frac{\partial C}{\partial t} + \nabla C \cdot \mathbf{w} = K_C \Delta C + Src - Snk. \tag{5}$$

where K_C is the diffusion coefficient and Src and Snk are source and sink terms depending on forcing condition of atmosphere and deeper layers.

We have to determine which conservation equation should be used for better estimating the motion field:

- Luminance conservation,
- Mass conservation,
- Temperature or Chlorophyll conservation.

Concerning SST images: the mass conservation equation is not adapted, since it applies to densities, and should not be applied to a scalar variable like temperature, which is not homogeneous to a density. The rigorous mathematical framework is given by the advection-diffusion equation. If we use the Boussinesq approximation and consider that horizontal thermal diffusivity is very small, it is reasonable to consider the luminance conservation.

The main errors made when assuming luminance conservation on images, are related to the fact that we consider 2D equations in the image domain (rather than the theoretical 3D equations) and to the unavailable source and sink terms. However, these errors do not depend upon this particular equation and are inherent to the image context, whatever the conservation equation used.

Selection of points verifying the conservation equation We cannot expect that the luminance equation applies on all the image data for the following reasons:

- On specific structures, luminance conservation cannot be verified on image data because of a specific configuration of the motion which prevents its observation. This happens when the motion is perpendicular to the image gradient: in such a configuration, it does not make sense to solve the conservation equation since it is not observable from the image. These structures must be masked prior to the motion estimation process.
- There are a lot of locations where image data do not bring information on motion beacuse of the lack of image tracers (e.g. spatial gradient and temporal derivatives vanish).

– There are finally locations where image data allow for motion observation, but where the conservation equation is not well verified, for instance because we do not account for source and sink terms.

Our aim will then be to select points, where the conservation equation is verified, and to use these points for reconstructing the motion field over all the domain by means of a regularization process as detailed in 3.2. For that purpose, we must be able:

– To discard pixels belonging to structures that obviously cannot verify the conservation equation on image data: this requires a specific modeling of these structures and their extraction from the image.
– To select among the remaining pixels those verifying the conservation equation: by eliminating pixels with a high value of the residual $(\nabla I.\mathbf{w} + I_t)^2$ and those with no image information (∇I and $I_t \simeq 0$). This is a pixel-level process based on local criteria such as spatial gradient and temporal derivatives.

We first discuss the problem of the specific structures we are trying to mask, then we discuss the image criteria used to select points verifying the conservation equation.

The structures for which luminance conservation cannot be verified on image data have the following characteristics:

– the velocity and image gradient are perpendicular.
– they are stable and do not undergo a global motion.

As a matter of fact, it should be reminded that the conservation equation only brings information on one component of the motion: its projection onto the image gradient (see equation 2). If the two above conditions are met, then we cannot expect finding information on motion from the image data. After analysis of the OPA sequence, we find that this situation is met with specific structures called filaments. Filaments are elongated structures, rather stable in time, but with important inner motion oriented in the direction of the elongation, thus perpendicular to the gradient (figure 4).

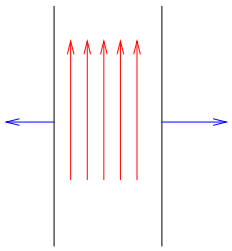

Fig. 4. Filaments: the velocity (red arrows) is orthogonal to the image gradient (blue arrows).

Our proposed approach for filament detection is first based on their elongated shape: we apply tools issued from mathematical morphology (peak and valley operators), that will detect shapes with a maximal width and that are brighter (peak) or darker (valley) than the background. These two will result in all shapes with limited width, as depicted on figure 5. The resulting detected shapes are

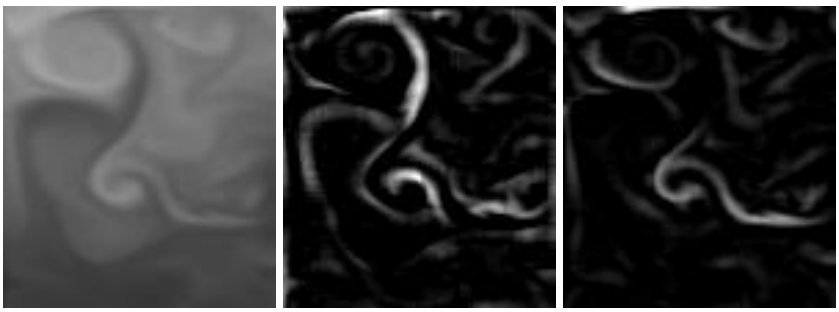

Fig. 5. Left to right: test image (extracted from OPA sequence), result of the peak operator, result of the valley operator.

further filtered to retain only those with sufficient elongation. This is performed by computing their inerty matrix, and thresholding the ratio of the two eigenvalues (see figure 6). The last criteria used concerns the structures' global motion:

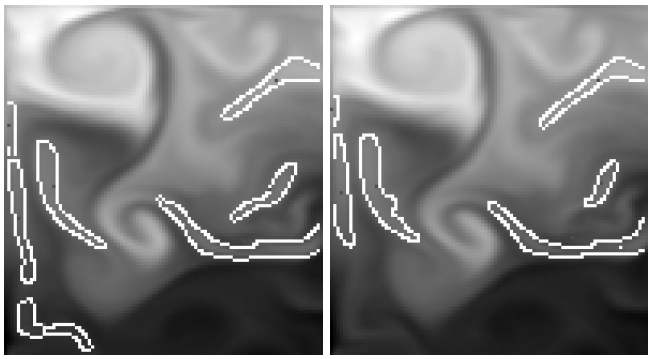

Fig. 6. White contours: contours of the structures detected with the peak operator and with sufficient elongation, computed on frames 52 and 53.

we only want to retain stable structures. Detected structures in two consecutive frames are matched and their global motion computed. If this motion is small enough, then the structure is considered as a filament and discarded from the motion estimation process (see figure 7 for results examples).

Fig. 7. In red: elongated structures (from both peak and valley images) considered to be filaments in frame 52.

Having discarded structures where motion is orthogonal to the gradient, we now have to consider the remaining pixels and to retain only those with enough image information and verifying the conservation equation. For that purpose we have analysed the residual of the conservation equation using the OPA motion field $\mathbf{w}_M$, in order to investigate where the conservation equation is verified, and we have tuned local criteria in order to automatically find these points from the image data.

- A threshold applied on the *motion index* (ratio between temporal derivative and spatial gradient magnitude) provides pixels where there is enough information in the image to solve the conservation equation (i.e. we don't try to solve $0.\mathbf{w} = 0$).
- The analysis of the OPA motion field $\mathbf{w}_M$ shows that points with low residual of the conservation equation have a high spatial gradient magnitude. Reciprocally, only points sufficiently close to a contour (i.e. a local maximum of the spatial gradient magnitude) have a low residual, and thus verify the conservation equation.

Summarising: the selection of points verifying the conservation equation is based on a three-steps process:

- Discarding structures which specific motion configuration (orthogonal to the contours) prevents its observation from image data. These structures are identified as filaments, and a specific detection procedure is proposed. These structures are masked and discarded from the motion estimation process.
- Filtering pixels where image information is not sufficient. This is done by thresholding the motion index.
- Finally, detecting among the remainder points with low residual, by selecting points with high gradient magnitude in the vicinity of a contour.

This process results in the selection of initial points, from which the motion is computed and reconstructed over the whole image domain by applying a regularisation process.

Which regularity equation? In the context of computer vision different equations have been extensively studied:

- $L1$ [10]:

$$E_2^{(1)}(\mathbf{w}) = \int_{image} \mid \nabla \mathbf{w} \mid . \tag{6}$$

- $L2$ [18]:

$$E_2^{(2)}(\mathbf{w}) = \int_{image} \|\nabla \mathbf{w}\|^2. \tag{7}$$

- 1st order div/curl [2, 16, 32]:

$$E_2^{(3)}(\mathbf{w}) = \int_{image} \alpha \|\mathrm{div}\mathbf{w}\|^2 + \beta \|\mathrm{curl}\mathbf{w}\|^2. \tag{8}$$

- 2nd order div/curl [2, 12, 16, 30]:

$$E_2^{(4)}(\mathbf{w}) = \int_{image} \alpha \|\nabla \mathrm{div}\mathbf{w}\|^2 + \beta \|\nabla \mathrm{curl}\mathbf{w}\|^2. \tag{9}$$

These energy values will be computed for the OPA model velocity field $\mathbf{w}_M$ (displayed on figure 2) as previously explained. The energy function providing the lowest value on this simulated field is selected for further estimation on satellite data.

Results show that the 2nd order div-curl regularization is best verified by OPA motion field. This is in agreement with experiments made in the meteorological domain by several authors [2, 12, 30]. The α and β coefficients must be tuned so as to strongly penalise divergent motion fields and to relax vorticity, as expected because of the use of Boussinesq approximation.

Results on apparent motion estimation The following results are computed on SST images. As explained above, the motion field is computed according to the luminance conservation hypothesis and the 2nd order div-curl regularity constraint.

Moreover, a point selection process is applied, providing points where the conservation hypothesis is best verified. This set of points is usually sparse and prevent us from using cost functions defined on the whole image data, as performed by [12, 18]. This led us to apply a vector spline approach, introduced by [2] for reconstructing sparse vector data using the 2nd order div-curl regularity. This method has been extended by [30], in order to deal with projected vectors, which is our case since we only observe the projection of the velocity on the image gradient (the normal velocity). As a result, we obtain a motion field verifying 2nd order div-curl regularity, and which normal velocity equals the normal velocity observed at the initially selected points.

Figure 8 displays the set of initial points, the estimated motion $\mathbf{w}$, and the OPA-modeled motion $\mathbf{w}_M$. It can be seen that the vortex (A) and the double

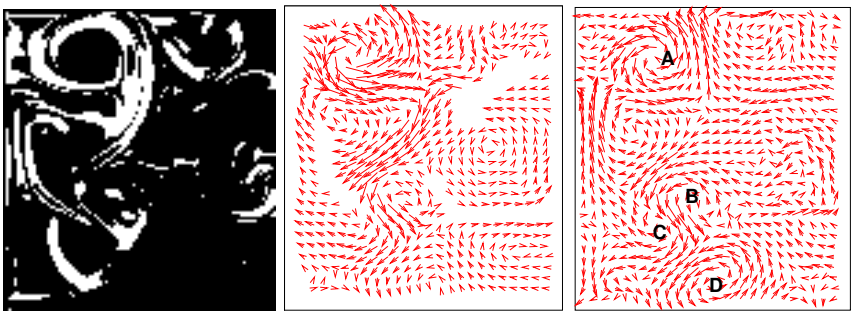

Fig. 8. Set of initial points in white (left), estimated motion (middle), real motion (right).

vortices (B, C) are quite well recovered. The vortex (D) in the dark-cold region cannot be recovered because there is not enough image information in this area. Areas where no motion information is provided correspond to the filaments detected and masked prior to motion estimation.

The next subsection is dealing with detection and tracking of specific structures (eddies), with the objective of computing Lagrangian trajectories.

3.3 Structure detection of tracking for trajectories computation

In this subsection we address the segmentation and tracking of specific structures (eddies), with the following motivation: when tracking these structures all along the image sequence, one is able to infer Lagrangian trajectories, an information which can also be assimilated within oceanographic models.

Segmenting and tracking a specific type of structure in an image sequence requires a proper modelling of its image characteristics, in order to detect it in a robust manner.

Eddies, have a circular shape with concentric lines of approximately constant grey level, and high contrast at the edges. See figure 9 for an example of such a structure.

The circular shape of the structures of interest, as well as the constant contrast along their edges, indicate that a contour based segmentation and tracking process can be successfully applied. Active contour models, known as *snakes* [20], have proven their robustness in the context of oceanographic structure segmentation and tracking [17]. Snakes are parameterized curves $f(s)$ defined for a real parameter $s \in S$, that minimize a criterion stating that:

- The curve undergoes regularity requirements: this is the internal energy, and it expresses the fact that we are looking for smooth enough curves. This term is most often expressed as constraints applied on its elasticity and rigidity.
- The curve should lie in the vicinity of locations of maximal contrast: this criterion expresses the data confidence, and is computed from a potential

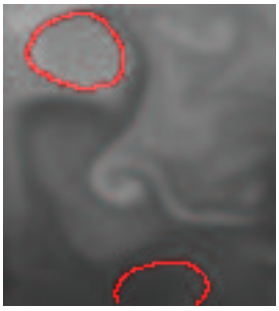

Fig. 9. Examples of eddies in the OPA sequence.

P defined over the image domain. This potential should be minimal at the vicinity of the structures of interest. A classical definition is: $P = -\|\nabla I\|^2$.

Altogether, the classical formulation of snakes leads to the minimisation of the following energy functional $E(f)$:

$$\min E(f) = \int_S \alpha(\frac{\partial f}{\partial s})^2 + \beta(\frac{\partial^2 f}{\partial^2 s})ds + \lambda \int_S P(f(s))ds \tag{10}$$

The parameters α, β and λ tune the importance of the elasticity, rigidity and data confidence respectively.

An alternative to this regularity, very adapted to quasi circular shapes, is to state that the curve belongs to a predefined mathematical class of curves Q, such as quadrics or hyperquadrics [11]: the snake must only minimise the data confidence criterion, as long as f belongs to this specific family of curves.

$$\min \int_S P(f(s))ds \text{ and } f \in Q \tag{11}$$

where Q is the ensemble of hyperquadrics.

The process of computing the snake then relies on the minimisation of the energy functional $E(f)$. Usually we are only interested in a local minimum, and we have to start from an initial guess f_0 not too far from the contour of interest. This initial guess is user-defined. E is then minimised by means of a gradient descent algorithm.

Snakes can be used for efficiently tracking structures in a quasi automatic fashion: the snake describing the structure in the previous frame is used as initial guess for the current one. If the structure's displacement is small enough between consecutive frames, then the energy minimisation process can be succesfully applied on each frame of the sequence. The human intervention thus only concerns the initialisation of the snake at the beginning of the sequence. Results of eddy tracking using snakes are depicted on figure 10.

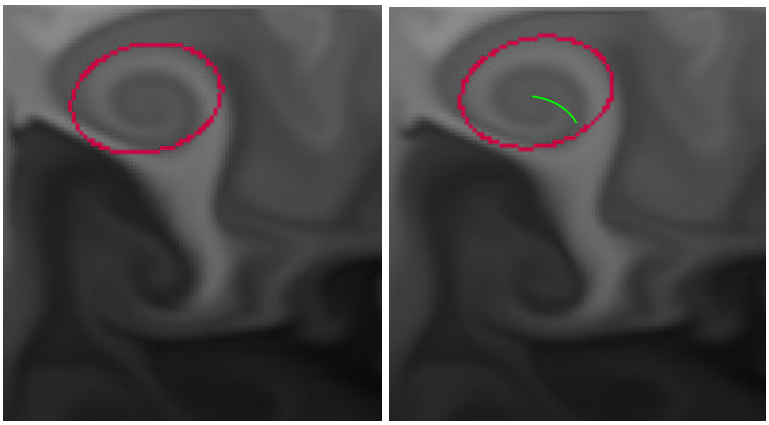

Fig. 10. Eddy segmentation by snakes (red curves) performed between frames 24 to 30 of the OPA sequence. The trajectory (depicted in green) of the center could be assimilated in a Lagrangian framework.

4 Conclusion

This paper aims at presenting the potential of satellite images for assimilation within geophysical models, focusing on the oceanographic application. We have to extract information (apparent motion, structures, ...) and find how to assimilate it in the models. We also explained how the final use of image processing results, which is assimilation and not visualization, is modifying the way we are defining processing algorithms. Endly, we explained how we can use the available information on satellite data acquisition on the studied phenomena (here oceanic circulation) within the algorithms. For example, we extensively discussed how to choose the conservation equation and the regularity constraint for the problem of apparent motion computation. We illustrate these points with synthetic data obtained by an oceanic model in order to be able to validate our assumptions.

References

1. L. Alvarez, J. Weickert, and J. Sanchez. Reliable estimation of dense optical flow fields with large displacements. *IJCV*, 39(1):41–56, August 2000.
2. L. Amodei. A vector spline approximation. *Journal of approximation theory*, 67:51–79, 1991.
3. E. Arnaud, E. Mémin, and B. Cernuschi-Frias. Conditional filters for image sequence based tracking - application to point tracking. *IEEE Trans. of Image Processing*, 2004.
4. J. Barron, D. Fleet, and S. Beauchemin. Performance of optical flow techniques. *International Journal of Computer Vision*, 12(1):43–77, 1994.
5. S.S. Beauchemin and J.L. Barron. The computation of optical flow. *Surveys*, 27(3):433–467, September 1995.

6. D. Béréziat, I. Herlin, and L. Younes. A generalized optical flow constraint and its physical interpretation. In *Proceedings of CVPR'2000*, 2000.
7. E. Blayo. Modélisation numérique et assimilation de données en océanographie - Habilitation à Diriger des Recherches, 2002.
8. D. Béréziat. *Estimation et suivi de structures déformables en mouvement: application à la météorologie*. PhD thesis, Université de Paris Sud - Paris XI, 1999.
9. I. Cohen. Nonlinear variational method for optical flow computation. *Proceedings of the 8th SCIA*, page 523, June 1993.
10. I. Cohen and I. Herlin. Optical flow and phase portrait methods for environmental satellite image sequences. In *ECCV*, volume 2, page 141, 1996.
11. Isaac Cohen and Laurent Cohen. A hyperquadric model for 2-D and 3-D data fitting. In *12th International Conference on Pattern Recognition*, Jerusalem, October 1994. IEEE-IAPR.
12. T. Corpetti. *Estimation et analyse de champs denses de vitesses d'écoulements fluides*. PhD thesis, Université de Rennes I, July 2002.
13. T. Corpetti, E. Mémin, and P. Pérez. Dense estimation of fluid flows. *IEEE Transactions on Pattern Analysis and Machine Intelligence*, 24(3):365–380, March 2002.
14. S. Durbiano, E. Blayo, J. Verron, J. Blum, and F. Le Dimet. A reduced order strategy for 4D-var ocean data assimilation. *Quarterly Journal of the Royal Meteorological Society*, 2002.
15. K.J. Flynn. A mechanistic model for describing dynamic multi-nutrient, light, temperature interactions in phytoplankton. *Journal of Plankton Research*, 23:977–997, 2001.
16. S. Gupta and J. Prince. Stochastic models for div-curl optical flow methods, 1996.
17. I. Herlin, I. Cohen, and S. Bouzidi. Image processing for sequence of oceanographic images. *The Journal of Visualization and Computer Animation*, 7:169–176, 1996.
18. B.K.P. Horn and B.G. Schunk. Determining optical flow. *Artificial Intelligence*, Vol 17:185–203, 1981.
19. Y Junqing and F.-X. Le Dimet. Variational data assimilation in the transport of sediment in river. *Science in China (Seres D)*, 41:473–485, 1998.
20. Michael Kass, Andrew Witkin, and Demetri Terzopoulos. Snakes: Active contour models. *International Journal of Computer Vision*, 1:321–331, 1987.
21. F.-X. Le Dimet and O. Talagrand. Variational algorithms for analysis and assimilation of meteorological observations: Theoretical aspects., 2002. Tellus, 38A, 97-110.
22. M. Levy, M. Gavart, L. Memery, G. Caniaux, and A. Paci. A 4D-mesoscale map of the spring bloom in the POMME experiment (Northeast Atlantic): results of a prognostic model. *Journal of Geophysical Research*, 2004.
23. G. Madec, M. Imbard, and C. Lévy. *OPA 8.1 Ocean General Circulation Model Reference Manual*. Institut Pierre Simon Laplace, Paris, 1999. Notes scientifiques du pôle modélisation.
24. A. Mitiche and P. Bouthemy. Computation and analysis of image motion: A synopsis of current problems and methods. *International Journal of Computer Vision*, Vol 19(1):29–55, 1996.
25. E. Mémin and P. Pérez. A multigrid approach to hierarchical motion estimation. In *Proc. Int. Conf. on Computer Vision, ICCV'98*, pages 933–938, Bombay, India, January 1998.
26. E. Mémin and P. Pérez. Optical flow estimation and object-based segmentation with robust techniques. *IEEE Trans. on Image Processing*, 7(5):703–719, May 1998.

27. E. Mémin and P. Pérez. Hierarchical estimation and segmentation of dense motion fields. *Int. Journal of Computer Vision*, 46(2):129–155, February 2002.
28. H.H. Nagel. Displacement vectors derived from second-order intensity variations in image sequences. *Computer Graphics Image Processing*, 21:85–117, 1983.
29. P. Saturette and P. Arbogast. Water vapour image: a tool for allowing the forecaster to monitor and improve the model initial state. In *Proceedings of the EUMETSAT 2002 meteorological satellite conference*, Dublin, September 2002.
30. D. Suter. Motion estimation and vector splines. In *CVPR94*, 1994.
31. F.-X. Vieux, B. Le Dimet and D. Armand. Inverse problem formulation for spatially distributed river basin. *Annales Geophysicae*, 16:501–509, 1998.
32. X. Vigan, C. Provost, R. Bleck, and P. Courtier. Sea surface velocities from Sea Surface Temperature image sequences. *Journal of Geophysical Research*, August 2000.
33. R.P. Wildes and M.J. Amabile. Physically based fluid flow recovery from image sequences. In *CVPR97*, pages 969–975, 1997.